Biol Cybern (2008) 98:491–507
DOI 10.1007/s00422-008-0217-1

ORIGINAL PAPER

Biological Cybernetics

# Design principles of sensory processing in cerebellum-like structures

## Early stage processing of electrosensory and auditory objects

**Patrick D. Roberts · Christine V. Portfors**

Received: 26 October 2007 / Accepted: 3 January 2008


**Abstract** Cerebellum-like structures are compared for two sensory systems: electrosensory and auditory. The electrosensory lateral line lobe of mormyrid electric fish is reviewed and the neural representation of electrosensory objects in this structure is modeled and discussed. The dorsal cochlear nucleus in the auditory brainstem of mammals is reviewed and new data are presented that characterize the responses of neurons in this structure in the mouse. Similarities between the electrosensory and auditory cerebellum-like structures are shown, in particular adaptive processes that may reduce responses to predictable stimuli. We suggest that the differences in the types of sensory objects may drive the differences in the anatomical and physiological characteristics of these two cerebellum-like structures.

**Keywords** Mormyrid · Electrosensory · Mouse · Auditory · Purkinje cell · Cartwheel cell · Plasticity

## 1 Introduction

Object identification and localization requires the nervous system to process streams of sensory information and quickly analyze sensory scenes. Fast localization of objects can be essential to the survival of an animal. Thus, it is paramount that features specific to a particular object are analyzed at the earliest stages of sensory processing. However, to localize an object, clear identification of sensory features (Rogers and Butler 1992) must be extracted from the background noise of the environment, and the distinction between noise and interesting objects is dependent on past experiences and present goals of the animal.

In the present article, we will restrict our discussion to the commonalities and differences in processing information in two sensory modalities: electrosensory and auditory. One commonality between these sensory modalities appears to be anatomical; their sensory afferents project to the central nervous system via the eighth cranial nerve. A second anatomical commonality is that the afferents project to a cerebellum-like structure for an initial stage of processing.

Cerebellum-like structures are so-called because of their anatomical resemblance to the cerebellum (Fig. 1). These structures are characterized by a laminar organization with a layer of principal cells that possess extensive apical dendrites. These dendrites receive synaptic inputs from a large number of parallel fibers in a molecular layer. The cerebellum proper has a layer of Purkinje cells that receive inputs from up to 200,000 parallel fibers (Albus 1971; Harvey and Napper 1991). The Purkinje cells project to the cerebellar nuclei and inhibitory postsynaptic currents in neurons of the cerebellar nuclei are caused by axonal, simple-spikes from Purkinje cells. An additional input to Purkinje cells is from a climbing fiber that causes a large depolarization of the dendrites (complex spike) with every presynaptic spike.

An association between the complex spike and parallel fiber spikes leads to long-term depression (LTD) of the parallel fiber synaptic current. A class of theories on cerebellar function (Albus 1971; Marr 1969) presumes that the parallel fibers provide context information that is sculpted by climbing fiber activity to generate the temporal patterns of

This research is supported in part by National Science Foundation Grant No. IOB-0445648 to PDR and IOS-0620560 to CVP.

P. D. Roberts (✉)
Neurological Sciences Institute, Oregon Health & Sciences University, Beaverton, OR 97006, USA
e-mail: robertpa@ohsu.edu

C. V. Portfors
School of Biological Sciences, Washington State University, Vancouver, WA 98686, USA

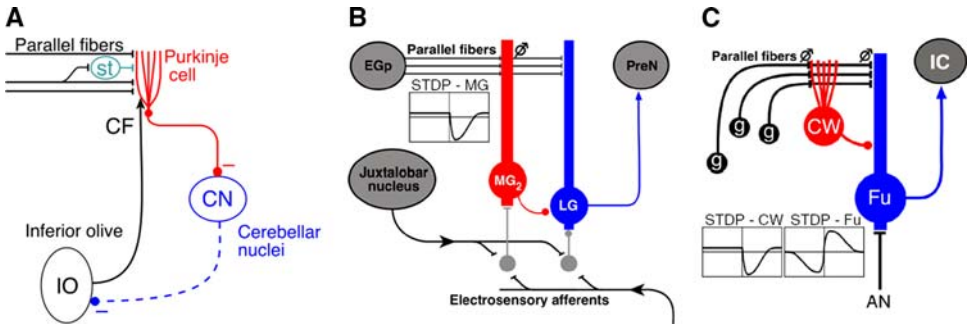


**Fig. 1** *Cerebellum-like structures.* **a** A simplified circuit diagram of the cerebellum. Purkinje cells are contacted by parallel fibers and inhibitory stellate cells (st), and project with inhibitory inputs to the cerebellar nuclei (CN). One climbing fiber (CF) excites each Purkinje cell and they originate in the inferior (IO). There is an inhibitory projection from the cerebellar nuclei to the inferior olive, but the functional role is unclear. **b** The cerebellum-like electrosensory lateral line lobe (ELL) of mormyrid electric fish. Parallel fibers arise from granule cells in the eminentia granularis posterior (EGp) and contact the Purkinje-like medium ganglion cells ($MG_1$ & $MG_2$) and the efferent cells (large ganglion, LG and large fusiform, LF). The MG cells inhibit the efferent cells. These cell types also receive EOD command timing information from the juxtalobar nucleus and electrosensory afferent inputs. The efferent cells project to the preementialis nucleus (PreN). The inset shows the STDP learning rule with synaptic change as a function of time between the pre- and postsynaptic spikes. **c** The cerebellum-like dorsal cochlear nucleus in the mammalian brainstem. Parallel fibers that arise from granule cells (g) throughout the DCN contact the Purkinje-like cartwheel cells (CW) and the efferent fusiform (Fu) cells. The fusiform cells project to the inferior colliculus. Insets show the STDP learning rules for both the CW cells and the Fu cells

Purkinje cell simple-spike output. Unfortunately, the precise timing relation between the complex spike and the parallel fiber spike that maximizes LTD is not known because of discrepancies between studies (Karachot et al. 1994; Chen and Thompson 1995; Linden and Connor 1993; Lev-Ram et al. 1995), but recent studies are pointing in the direction that the interval of maximal LTD occurs when the complex spike follows the parallel fiber spike (Lev-Ram et al. 2002; Coesmans et al. 2004; Roberts 2007), and the LTD can be reversed by long-term potentiation. Fortunately, the exact timing has been well-characterized in the following cerebellum-like structures.

Electrosensory information is initially processed by the electrosensory lateral line lobe (ELL), a cerebellum-like structure in the hindbrain of mormyrid electric fish. This structure has a layer of Purkinje-like, medium ganglion (MG) cells that receive parallel fiber inputs, and these MG cells inhibit the efferent cells of the ELL. Like Purkinje cells, MG cells have two types of spikes: broad, dendritic spikes and small, axonal spikes. However, the dendritic spikes are not generated by an external nucleus, but are generated by the depolarization state of the Purkinje-like cell itself. As in the cerebellum, the dendritic spikes are the postsynaptic event that is associated with parallel fiber spikes to result in LTD (Bell et al. 1997b; Han et al. 2000). In the next section, we will propose that the functional consequence of this synaptic plasticity is to reduce the sensory consequences of predictable events such as motor actions of the fish.

The second cerebellum-like structure that will be discussed is the dorsal cochlear nucleus (DCN) in the mammalian brain stem, an initial site of auditory processing. In the DCN, the Purkinje-like cells are cartwheel cells, and like MG cells, they generate their own dendritic spikes. An association between the dendritic, complex spikes leads to LTD (Fujino and Oertel 2003; Tzounopoulos et al. 2004), and the cartwheel cells inhibit the efferent cells on the DCN (Golding and Oertel 1997). The DCN is likely an adaptive filter like the ELL (Oertel and Young 2004), but the relationship to motor activity is not as straight forward as with the electrosensory system.

The ELL and DCN are very similar structures in both anatomy and physiology, and possibly even function. However, there are very important differences that may be related to the types of objects that are detected by each sensory modality. Electrosensory objects are spatially extended in three dimensions, and are projected onto the two-dimensional surface of the fish's skin. In contrast, auditory objects are essentially embedded in a pressure wave that is projected onto frequency and time dimensions by the cochlea, the auditory end-organ. These differences in the nature of the objects that each sensory system is attempting to identify and localize may explain the differences that we find when comparing the two cerebellum-like structures.

The approach that we will use to explore the differences between these structures is through mathematical modeling of the neural activity. Models of sensory adaptation that have been developed in each of these sensory systems to yield insights into general principles of learning in biological systems, insights that will be applied to our questions about how the early stages of sensory processing adapt to critical features of auditory objects. In the next section, we discuss the electrosensory adaptation system, and make comparisons with the auditory system in following sections.

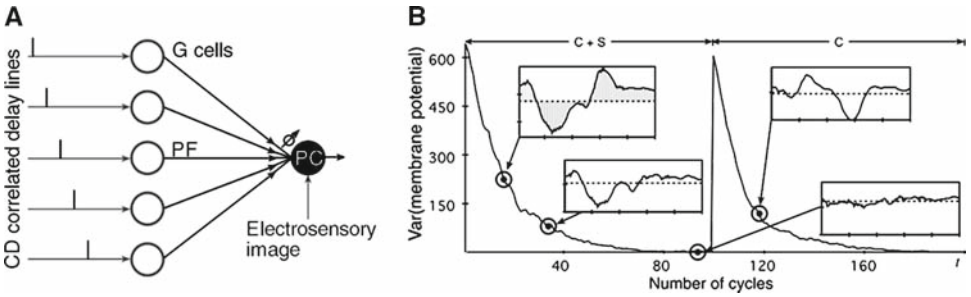


**Fig. 2** *Model of the electrosensory lateral line lobe (ELL) that cancels predictable electrosensory images.* **a** The electric organ corollary discharge (CD) signals enter the ELL through the EGp that contains granule cells (G cells) giving rise to parallel fibers responding as tapped delay lines following the CD. Parallel fibers (PF) synapses excite Purkinje-like cells (PC). Primary afferent fibers from electrosensory receptors enter the ELL and transmit temporal sensory pattern to PC. STDP at the PF synapse onto PC causes the output to adapt to the temporal pattern of the electrosensory image. **b** Simulated time evolution of adaptive response as measured by the variance of the model membrane potential versus the number of EOD cycle. For the first 100 EOD cycles, the command signal is paired with the sensory input (C+S), then the command cycle is presented alone **c**. Insets show the model's membrane potential during representative EOD-cycles

## 2 Expectation cancellation in mormyrid electric fish

A striking example of adaptive processing of spatiotemporal sensory patterns is found in the primary electrosensory processing system of mormyrid electric fish. The mormyrid electric fish senses its environment by emitting an electric organ discharge (EOD) and detecting the perturbations that nearby objects cause in the self-generated electric field. The fish also detects low-frequency, externally generated electric fields. However, the electroreceptors that are sensitive to external signals also respond to the fish's own EOD so that the EOD interferes with the detection of external sources. Since the fish generates the motor command for each EOD, the reafferent sensory signal is predictable. Mormyrids have developed a mechanism to *cancel predictable electrosensory signals so that the fish is exquisitely sensitive to novel electrical activity in its environment.*

Electrosensory information is transferred from the skin to the cortex of the ELL by electrosensory afferents. Motor information is also transferred to the ELL indicating *when* an EOD has taken place. These motor signals are called electric organ *corollary discharge* (CD) signals and are time-locked with the EOD motor command which elicits the EOD. A granule cell layer receives corollary discharge signals at various delays following the EOD (Bell et al. 1992) and the granule cells project to Purkinje-like cells via parallel fibers (Fig. 2a). Purkinje-like cells also receive electrosensory input from the periphery via interneurons in the deep layers of ELL. Repeated presentation of an electrosensory stimulus that is correlated with the CD results in the cancellation of the Purkinje-like cell's predictable response to the sensory stimulus (Bell et al. 1993).

Spike-timing dependent plasticity (STDP) (Abbott and Nelson 2000) at the parallel fiber synapse depresses the synapse after pairings in which a dendritic spike was evoked between 0 and 60 ms after the onset of the parallel fiber postsynaptic potential, while pairings at all other delays yield potentiation (Bell et al. 1993, 1997b). The plasticity of ELL cells observed at the systems level (Bell et al. 1993) has been shown to emerge from the learning rule measured in vitro (Roberts and Bell 2000; Williams et al. 2003). Remarkably, the modeling studies demonstrate that the STDP learning rule measured in vitro is optimal for cancellation of sensory images in the whole fish (Fig. 2b).

Two critical components of the model are necessary for cancellation of sensory images. One component is that the parallel fibers deliver a series of delayed postsynaptic potentials (delay lines) with respect to the EOD. The delay lines provide the necessary temporal structure needed for sensory image cancellation to be sculpted out of the parallel-fiber spikes. The second critical component is a synaptic learning rule that drives the Purkinje-like cell to an equilibrium during the correlated input. This second requirement is satisfied by the STDP learning rule in the mormyrid fish, but any synaptic adaptation mechanisms that drive the output neuron's membrane potential to an equilibrium could be used to model similar cancellations of predictable signals, as demonstrated in elasmobranchs (Nelson and Paulin 1995) and the cerebellum (Medina and Mauk 2000; Roberts 2007).

The equilibrium of the learning dynamics is constant for the passive electrosensory system. However, in the active electrosensory system, the dendritic spike threshold of the Purkinje-like neurons is modified so that the equilibrium of the learning dynamics is not constant throughout the EOD cycle (Roberts et al. 2006a; Sawtell et al. 2007). The result is that the dynamics of the STDP learning rule drive the Purkinje-like neurons to burst during a critical time following the EOD to control the output neurons' response to electrosensory signals. This adaptive control of the ELL output will presumably cancel expected sensory patterns that

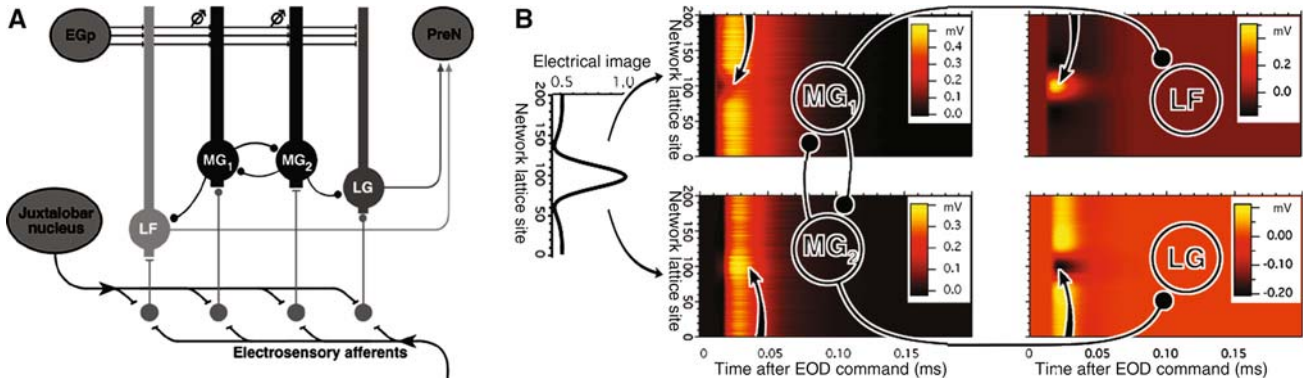


**Fig. 3** *One-dimensional network model of ELL.* **a** Model connectivity between cell types in ELL. **b** A chain of 800 neurons is represented on a lattice where 4 cells (1 of each type: MG1, MG2, LF, LG) occupy each lattice site. The neurons are synaptically coupled as shown by the schematic overlay. The electrical image (left) corresponds to a conductive object placed near the skin. The model predicts the average membrane potential (color scale) for each cell type at each lattice site during the first 200 ms following the EOD command. The model is then used to predict the pattern of the network activity during high EOD rate and object movements of probing behavior. The predicted membrane potential of efferent cells (LF and LG) is used to calculate the predicted spike output rate of the ELL network. Intracellular recordings of each cell type during slow EOD rates are used to fit the parameters of the model. *Arrows* correspond to the cell that represents the activity of the empirical recording

are encoded in the precise spike timings during each burst.

### 2.1 Spatial localization of electrosensory objects

Lateral connections in ELL affect the response of neurons to the presence of 3-D objects. Because of the "Mexican hat" nature of the electric images (Caputi et al. 1998), a given neuron population will experience sequences of excitatory and inhibitory influences during object interference with the field strength near the skin. This characterization of the input to ELL determines the dynamic responses of neurons in ELL to the projection of electric images on different parts on the electrosensory surface.

The effects of lateral connectivity arise from the mutual inhibitory connections between MG cells and their connection to efferent cells (Fig. 3). We hypothesize that the center-surround receptive fields of neurons will superimpose on the center-surround nature of the Mexican hat electric image. Using a network model that was tuned with data from point-stimuli (Mohr et al. 2002a,b), we predict the sensory image as represented by the network of LF and LG cells for electrical patterns encode images of novel objects.

*Model of spatiotemporal responses to objects.* Let $\mathbf{y}$ be a location on the skin, and we have assumed that the mormyromast afferent projections are somatotopic so that there is a mapping from any region on the skin ($\mathbf{y}$) to a region in ELL ($\mathbf{x}$) where $\mathbf{x}$ is a location in a specified zone (MZ or DLZ) of the ELL. For our present example shown in Fig. 3, we restrict our attention to the 1-dimensional case.

The *spike-probability function* for an LF cell located at $\mathbf{x}$ in the ELL is denoted by $P_{LF}(\mathbf{x}, t, n)$, where $t$ is the time following the command during an EOD cycle, and $n$ indexes which EOD cycle. Likewise for LG cells, $P_{LG}(\mathbf{x}, t, n)$, $\mathrm{MG}_1$ cells, $P_1(\mathbf{x}, t, n)$, and $\mathrm{MG}_2$ cells, $P_2(\mathbf{x}, t, n)$. Each spike-probability function is modeled as dependent on a membrane potential, $V(\mathbf{x}, t, n)$, that is defined as the sum of all synaptic inputs. Thus, the spike-probability function is

$$P_a(\mathbf{x}, t, n) = (1 + \exp[-\mu(V_a(\mathbf{x}, t, n) - \theta)])^{-1}, \qquad (1)$$

for each type of *principal cell* ($a = \mathrm{LF}$, LG, $\mathrm{MG}_1$, or $\mathrm{MG}_2$). The spike threshold, $\theta$, and noise parameter, $\mu$, are distinct for each cell type.

Excitatory synaptic inputs contribute to the membrane potential via postsynaptic-potential (PSP) kernels, $E(t) = (t/E)\exp(-t/E)$, that are based on normalized alpha functions in our example (Fig. 3). Parallel fiber inputs are represented by weighted postsynaptic-potential kernels where the weights are labeled by the time following the EOD command, $w(\mathbf{x}, t, n)$. For MG cells (but not LF and LG cells), the parallel fiber weights depend on the EOD cycle, $n$, because these synapses are plastic and follow an STDP learning rule. Stellate cell inputs to MG cells are also assumed to be plastic and contribute to the membrane potential with negative weights, $v(\mathbf{x}, t, n) < 0$. The stellate cells respond to parallel fiber input with an excitatory PSP that is then convolved with the inhibitory PSP kernel in the principal cell. We then approximate stellate filtering of the parallel fiber input with a "self-convolved" PSP kernel, $E^{(2)}(t) = E * E(t)$, where the asterisk represents convolution. Thus, the contribution to membrane potential from the molecular layer is expressed as $V_{mol}(\mathbf{x}, t, n) = w(\mathbf{x}, t, n) * E(t) + v(\mathbf{x}, t, n) * E^{(2)}(t)$ for MG cells, and the $n$-dependency of the weights are dropped for LF and LG cells.

Lateral connections between principal cells are a result of MG cell axons that terminate below the ganglion layer (Han et al. 1999). The spread of these inhibitory synaptic connections has been estimated by morphological studies of axons and dendrites of the principal cells (Han et al. 1999). The weight function is a Gaussian function of the location on the ELL,

$$W(\mathbf{x}) = u/\left(s\sqrt{\pi}\right)\exp[-(\mathbf{x}/s)^2].$$

Since MG cells are GABA-ergic, the weights are negative, $u < 0$.

Synaptic input from granular cells in the deep layers relays command signals from the juxtalobar nucleus and electrosensory afferents. For a constant sensory input, we denote the deep layer contribution to the membrane potential as $V_{deep}(\mathbf{x}, t) = V_{jln}(t) + V_{af}(\mathbf{x}, t)$. The afferent signal arrived at the principal cells after a chain of transformations:

Voltage across skin ($v(\mathbf{x})$)

- mormyromast afferent latency ($L(x) = L/v(\mathbf{x})$)
- granular cell spike probability ($P_G(\mathbf{x}, t)$)
- principal cell PSP ($D_a\, E * P_G(\mathbf{x}, t)$)

The granular cell response to the afferent spikes involves a function of the time difference between the EOD command, $\hat{t}_c$, and the afferent latency, $G_{af}(L(\mathbf{x}) - \hat{t}_c, t_i)$. We have assumed that the granular cells respond to a summation of EPSPs that cross a threshold. The granular cells that respond to juxtalobar nucleus input, $G_{jln}(t_i - \hat{t}_c)$, also contribute to the principal cell PSP. If $D_a$ is the weight of the deep-layer synaptic input, then the contribution to the membrane potential is $V_{deep}(\mathbf{x}, t) = D_a\, E * [G_{af}(L(\mathbf{x}) - \hat{t}_c, t_i) + G_{jln}(t_i - \hat{t}_c)]$. These functions have been fit to data that compared the PSP in principal cells for different delays between the EOD command and a sensory stimulus (Mohr et al. 2002a).

We then express the membrane potentials of the principal cells as

$$\begin{aligned} V_1(\mathbf{x}, t, n) &= W_{21}(\mathbf{x}) * (E(t) * P_2(\mathbf{x}, t, n)) \\ &\quad + V_1^{mol}(\mathbf{x}, t, n) + V_1^{deep}(\mathbf{x}, t) \qquad (2) \\ V_2(\mathbf{x}, t, n) &= W_{12}(\mathbf{x}) * (E(t) * P_1(\mathbf{x}, t, n)) \\ &\quad + V_2^{mol}(\mathbf{x}, t, n) + V_2^{deep}(\mathbf{x}, t) \qquad (3) \\ V_F(\mathbf{x}, t, n) &= W_{1F}(\mathbf{x}) * (E(t) * P_1(\mathbf{x}, t, n)) \\ &\quad + V_F^{mol}(\mathbf{x}, t) + V_F^{deep}(\mathbf{x}, t) \qquad (4) \\ V_G(\mathbf{x}, t, n) &= W_{2G}(\mathbf{x}) * (E(t) * P_2(\mathbf{x}, t, n)) \\ &\quad + V_G^{mol}(\mathbf{x}, t) + V_G^{deep}(\mathbf{x}, t) \qquad (5) \end{aligned}$$

where we made the approximation that all PSP were described by the same function.

The internal dynamics of the recurrent layer have been calculated using a perturbation expansion (Roberts 2004). The average membrane potential is represented by, $\langle V_a(\mathbf{x}, t, n)\rangle = v_a(\mathbf{x}, t, n) + W_{ab} * E * P_a(\mathbf{x}, t, n)$, where $v_a$ is the membrane potential of each neuron without the recurrent inputs in Eqs. 2 and 3.

We expand the spike probability functions in the high-noise limit, $\mu \approx 0$, and then we collect the terms to arrive at the synaptic loop-expansion (Roberts 2004),

$$\begin{aligned} \mathbf{P}_a(\mathbf{x}, t, n) &= \mathbf{p}_a(\mathbf{x}, t, n) + \sum_{K=1}^{\infty} \\ &\quad \times \left(\frac{\mu}{4}\right)^K \mathbf{W}^{(K)}(\mathbf{x}) * E^{(K)}(t) * \mathbf{p}_a(\mathbf{x}, t, n), \end{aligned} \qquad (6)$$

where $p_a(\mathbf{x}, t, n)$ is the spike probability vector without synaptic input from other elements of the recurrent layer. The loop-expansion formula (Eq. 6) converges for weak synaptic connections and high noise. We are justified in truncating the expansion (Roberts 2004) because both MG cell types respond to the command with an EPSP simultaneously implying that the system is in an asynchronous state.

Using the network model that is tuned with data from point-stimuli (Mohr et al. 2002a,b), we have predicted the image of a conductive object as represented by the network of LF and LG cells for electrical edge-images (Fig. 3b). Using data from recordings of the sensory response of single cells to similar edges recorded by our collaborators, we have quantified the average membrane potential and spike probability from electrophysiological recordings. Since the model contains a subset of the identified cell types of ELL, we expect that the differences between our prediction and the experimental results will inform us of which additional cell types must be added to our model to minimize any error in comparison with experimental results. However, this model does give an estimate of the encoding of objects as spike patterns across the surface of ELL.

### 2.2 The ELL as an adaptive filter for complex electrosensory stimuli

Assuming that the MG and efferent cells of ELL are tuned to a baseline of activity (Roberts et al. 2006a), the STDP learning rule will drive the system back to equilibrium after a prolonged exposure to a particular object. Thus, the system adapts to amplify novel electrosensory patterns (Bell 1989) and learns to ignore sensory images that do not change. This early stage of electrosensory processing is not "encoding" object features, but rather preparing the sensory image for more precise feature extraction further downstream. The example shown in Fig. 3b reveals object features that are modified by ELL processing. The lateral inhibitory nature

of the network amplifies the edges and sharpens the image. Coupled with synaptic plasticity at the parallel fiber synapse onto MG cells, the sharp image is predicted by the model to fade as the electrical perturbation is maintained over many cycles. Thus, novelty is both amplified and sharpened.

Amplification of novel objects could activate attention mechanisms to engage the fish in more detailed object identification and localization tasks. Similar to a searchlight of attention (Crick 1984) hypothesized for spatial sensory processing, but activated from the bottom up. The localization of the object requires further processing because only the 2-dimensional location is present in the activity patterns of the ELL. Ambiguities of the distance must be resolved using global information from the ELL's activity pattern (von der Emde et al. 1998).

Another essential function of ELL is to cancel the sensory consequences of the fishes own movements. For instance, the movement of the fish's tail will cause the baseline electric field strength on the skin to change in a complex manner (Caputi and Budelli 2006; Gomez et al. 2004). However, the sensory consequences of the tail movement will be correlated with proprioceptive information projected to the parallel fibers of ELL (Bell et al. 1992). Such cancellation of movement effects has been observed in other electroreceptive fish (Bell et al. 1997a; Bastian 1996; Bodznick et al. 1992; Montgomery and Bodznick 1994), and appears to be evident in the mormyrid ELL (Sawtell and Williams 2008).

## 3 A cerebellum-like structure for auditory processing

The dorsal cochlear nucleus (DCN) is one of the two initial sites of auditory processing in the mammalian brainstem. Along with receiving primary auditory inputs, the DCN receives additional ascending and descending auditory inputs and inputs from non-auditory sources. This convergence of information may be important for utilizing synaptic plasticity to alter auditory responses to expected stimuli. Quantifying neural responses to complex sounds in DCN can be compared with mechanistic models of DCN cell types to determine how DCN neurons respond to complex sounds. The effects of plasticity on auditory responses will then be predicted by our quantitative model to demonstrate how the DCN encodes auditory objects. The integration of empirical studies with mathematical modeling increases our understanding of how the DCN functions as an adaptive filter during sound processing.

### 3.1 The DCN is a cerebellum-like structure

The DCN is the most complex of the cochlear nuclei, and has been extensively studied both physiologically (Pfeiffer 1966; Evans and Nelson 1973; Godfrey et al. 1975; Kaltenbach and Saunders 1987; Young and Brownell 1976; Rhode and Smith 1986; Rhode and Kettner 1987) (see Young and Davis 2002 for review) and anatomically (Osen 1969; Rhode et al. 1983; Wouterlood and Mugnaini 1984; Wouterlood et al. 1984; Ryugo and Willard 1985; Smith and Rhode 1989; Berrebi and Mugnaini 1991). In this paper, we address the function of the DCN from the standpoint of its similarity to the cerebellum and cerebellum-like structures. In particular, our hypotheses are driven by similarities between the DCN and the cerebellum-like nuclei in fish (Bell et al. 1997a). In electric fish ELL, an anti-Hebbian form of synaptic plasticity cancels the expected features in sensory input (Bell 1981; Bell et al. 1997b; Roberts and Bell 2000). Similar synaptic plasticity has recently been shown in the DCN of mouse suggesting that similar adaptive mechanisms may exist in the two structures (Tzounopoulos et al. 2004). A major objective of this study has been to determine whether adaptation is present in DCN by examining adaptation of cartwheel cells in the DCN of an awake, listening mouse.

The output neurons of DCN (fusiform and giant cells) receive direct input from auditory nerve afferents and inputs from parallel fibers (Fig. 4a). Parallel fibers originate in the granule cell domain and synapse onto fusiform, cartwheel and giant cells in the superficial layer of DCN. The granule cells and their parallel fiber axons convey information from a wide range of auditory and non-auditory sources: the auditory cortex (Weedman and Ryugo 1996), the inferior colliculus (Caicedo and Herbert 1993; Schofield and Cant 1999), the dorsal column nuclei (Li and Mizuno 1997), the pontine nuclei (Ohlrogge et al. 2001), the trigeminal nucleus (Li and Mizuno 1997; Shore et al. 2000; Haenggeli et al. 2005), unmyelinated auditory nerve fibers (Brown et al. 1988), and the ventral cochlear nucleus (Golding et al. 1995). In addition, fusiform cells receive inhibitory input from cartwheel cells whose cell bodies reside in the molecular layer (Berrebi and Mugnaini 1991). Cartwheel cells do not receive primary afferents but are excited by parallel fibers, including fibers that carry auditory information (Parham et al. 2000). We have used mathematical models to develop the hypothesis that plasticity between parallel fibers and cartwheel cells leads to the cancellation of expected auditory patterns, and then tested that hypothesis using *in vivo* recordings of cartwheel cells.

There is compelling evidence of synaptic plasticity at several sites within the DCN (Fujino and Oertel 2003; Tzounopoulos et al. 2004). For example, in vitro studies have shown STDP in the mouse DCN that can strongly modify the synapses from parallel fibers onto cartwheel cells and fusiform cells (Tzounopoulos et al. 2004), and the STDP learning rules (Fig. 4b) have been well characterized. However, it is difficult to determine the effect, if any, that synaptic plasticity has on the information processing that takes place in the auditory pathway. Insights regarding the functional significance of this plasticity are best obtained through *in vivo*

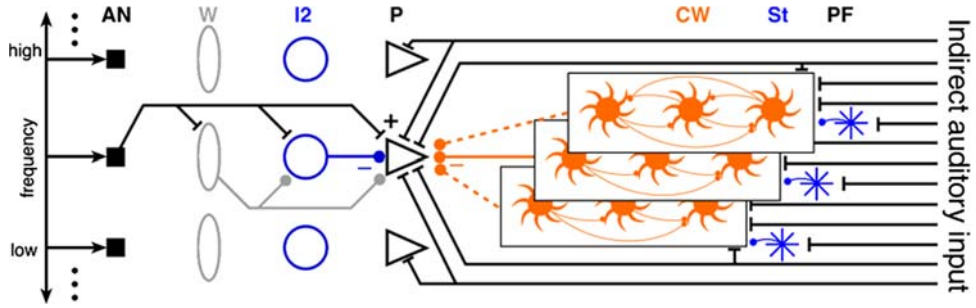


**Fig. 4** *Connectivity of DCN network model.* Our model of fusiform cell responses will extend previous research by combining our preliminary fusiform model (Module 1) with a population of model cartwheel cells (Module 2) (Portfors and Roberts 2007). Fusiform cells (P) are excited by the auditory nerve (AN) (Nelson and Carney 2004) and parallel fibers, and they are inhibited by wide-band inhibitory interneurons (W) and type II units (I2). The cartwheel cells will have response properties derived from experimental recordings, and inhibit fusiform cells via synaptic connections with glycinergic kinetics. In the extended model, the model cartwheel cells will be excited by indirect auditory pathways via parallel fibers (PF) and receive GABA-ergic synaptic inputs from stellate cells (St) and glycinergic inputs from other cartwheel cells. Cartwheel cells will be organized into isofrequency subpopulations (depicted by *layered boxes*) that that are reciprocally connected and converge onto similarly tuned fusiform cells. The extended model will predict responses of fusiform cells to auditory stimuli of longer duration than we used to tune our preliminary model due to the long latency responses of cartwheel cells

studies of mouse DCN where responses to natural auditory stimuli can be examined. The STDP learning rules have been formalized mathematically to predict how synaptic efficacy changes for a wide variety of spike patterns (Roberts and Bell 2002). The models that has been constructed incorporates our current understanding of STDP learning dynamics and tests how these dynamics affect auditory processing in the DCN. The objective of our model of cartwheel cell responses is to predict the effects of synaptic plasticity in DCN on the processing of complex sounds.

The STDP learning rule at the parallel fiber synapse onto cartwheel cells would cause a cancellation of expected stimuli if the parallel fibers carried timing information about the stimuli (Roberts and Bell 2002, 2000). The STDP learning rule at the parallel fiber synapse onto fusiform cells would lead to a linking of sensory events separated in time. Temporal correlations would cause a strengthening of a weak response to the stimulus if repeatedly paired with a second, later stimulus that evoked a response (Roberts and Bell 2002; Roberts 1999). However, because cartwheel cells inhibit fusiform cells (Fig. 4), the two types of learning rules interact to modulate the output of DCN neurons, and the adaptation of spectral–temporal responses of fusiform cells may be quite complex. Therefore, we have developed a mechanistic model to predict the responses of cartwheel *and* fusiform cells to vocalizations; sounds that have complex frequency and time structures. We then add a STDP learning rule into our mathematical models to predict how response properties of DCN output neurons changes after adaptation. We compared the model's predictions for adaptation of cartwheel cells to simple tone pairs with empirical data. The results have informed us about the mechanisms of adaptation to more complex sounds as they operate in the awake, listening animal.

### 3.2 The DCN as an adaptive filter for auditory stimuli

The function of the DCN as a filter for sound localization cues has been discussed extensively in the literature (Davis et al. 1996b; Ding et al. 1999; May 2000; Oertel and Young 2004; Reiss and Young 2005; Young et al. 1995; Young and Davis 2002; Zheng and Voigt 2006). Spectral cues from the head transfer function are thought to be combined in DCN with proprioception information to determine the location of a sound source. This filtering process is adaptive because the shape of the pinna, or the coding of proprioceptive information, could change through growth or injury. Behavioral studies using animals with lesions to the DCN (or output pathways) have suggested some role in sound localization (Thompson and Masterton 1978; Jenkins and Masterton 1982; May 2000), and the behavioral deficits were largest for orienting to the elevation of the stimulus. However, the lesion studies may be difficult to interpret, particularly because the DCN receives information from many parts of the brain. The DCN will therefore act as an adaptive filter to expect the auditory consequences of *any sensory event* (Oertel and Young 2004), and use that expectation to modify signals in the auditory pathway. Therefore, any sensory event that is consistently correlated with an auditory stimulus (Oertel and Young 2004; Shore 2005; Young and Davis 2002; Woody et al. 1992) could be used to filter auditory information in DCN.

In addition to filtering sound localization cues, the DCN may also be involved in echo suppression (Kaltenbach et al. 1993; Wickesberg and Oertel 1990), vocal auditory suppression (Shore 2005), or enhancement of auditory processing in the presence of background noise (Franosch et al. 2003; Frisina et al. 1994). The responses of cells in DCN to auditory stimuli have also been observed to change during classical

**Table 1** Response types of neurons recorded in awake mouse DCN

| Response type | Number recorded | Percent of total units | Percent without cartwheel cells | Median first spike latency (mean ±S.D.) ms | Mean threshold (S.D.) dB SPL |
|---|---|---|---|---|---|
| II | 14 | 18.2 | 25 | 8.3 (3.5) | 29.6 (12.4) |
| I/III | 4 | 5.2 | 7.1 | 11 (7.5) | 26.6 (19.4) |
| III | 29 | 37.6 | 51.8 | 11.5 (5.6) | 25.9 (14.2) |
| IV | 0 | 0 | 0 | N/A | N/A |
| Inhibited | 9 | 11.7 | 16.1 | | 32 (14.6) |
| Complex spiking | 21 | 27.3 | N/A | 30.8 (14.3) | 33.1 (11.1) |

conditioning (Beroukha et al. 1998; Woody et al. 1992) using an eye blink conditioning protocol. These conditioning results suggest that DCN enhances responses to important auditory objects leading to a better characterization and localization of objects in a noisy environment. The general function of the DCN may be to enhance behaviorally important auditory objects for better identification and tracking in complex auditory scenes.

## 4 Response properties of neurons in the DCN of the awake mouse

The results presented here represent recent experimental studies of the DCN. These results have provided a useful theoretical framework to explain how plasticity and network properties of the cartwheel cell layer affect the activity patterns of DCN output neurons. In the course of our studies, we have recorded 77 isolated single units in the DCN in our awake mouse preparations, and found type II, III and I/III response types, but no type IV responses, and found that cartwheel cells in our awake mouse preparation respond well to tones. Our mechanistic model of cartwheel cells explains temporal firing patterns (Portfors and Roberts 2007), and predicts adaptation due to spike timing-dependent plasticity (STDP) (Roberts et al. 2006b). We found that the predicted response from the model was similar to adaptation observed in an isolated cartwheel cell recorded from awake mouse DCN. We also found that cartwheel cells respond to mouse vocalizations so that they may participate in the analysis of complex sounds. In the following section, we will demonstrate the results from a model we developed to quantify how complex frequency interactions affect the responses of fusiform cells in DCN.

### 4.1 Frequency and temporal responses of DCN neurons in awake mouse

The purpose of this study was to determine what response types are in mouse DCN so that we can use these to identify cell types. We have recorded 77 well-isolated single units from the DCN of awake CBA/CaJ mice. Iontophoretic deposits of dyes (dextran conjugated rhodamine (fluororuby) or biotynilated dextran amine) confirmed that we can access the DCN with our micropipette recording electrodes using a dorsal approach through the cerebellum. Characteristic frequencies of the units ranged from 6–32 kHz. We recorded 21 complex spiking units that we categorized as cartwheel cells (Portfors and Roberts 2007), and 9 that we classified as "inhibited". All other units were classified into response types based on the well described response map scheme (Evans and Nelson 1973; Young and Brownell 1976; Young and Voigt 1982; Young 1984; Shofner and Young 1985; Davis et al. 1995, 1996a).

The majority of responses in awake mouse DCN were type III (Table 1 ). Figure 5a, b shows frequency tuning of a fusiform and a vertical cell. The top plots show response maps at three intensities and the bottom plots show spectral-temporal histograms. In this type of plot, both frequency and temporal information are retained with time on the $x$-axis and frequency of sound stimulation on the $y$-axis. Each row represents the post-stimulus time histogram (PSTH) for the corresponding frequency. The temporal firing patterns of awake mouse DCN units were similar to those previously reported (Rhode and Smith 1986). Of the 56 units that were not cartwheel cells, the majority ($n$=22; 28.6%) were choppers. These results indicate that the awake mouse DCN lacks Type IV responses but that other response properties are similar to those observed in cat and gerbil.

The 21 cartwheel cells had distinct temporal firing patterns compared to the 56 principal cells. Often the initial complex spike was followed by a pause and then a simple spike. This temporal firing pattern appears as a bimodal spike distribution in many cartwheel cells. Cartwheel cells also have long and variable latencies compared to other unit types in DCN. The mean (SD) latency of cartwheel cells was 30.8 ms (14.2 ms) compared to values between 8.3 ms (3.5 ms) and 11.5 ms (5.6 ms) for other unit types (Table 1). This longer latency corresponds well with cartwheel cells not receiving direct, afferent input from the auditory nerve.

Previous studies of cartwheel cells have suggested that cartwheel cells respond weakly to sound and often a best

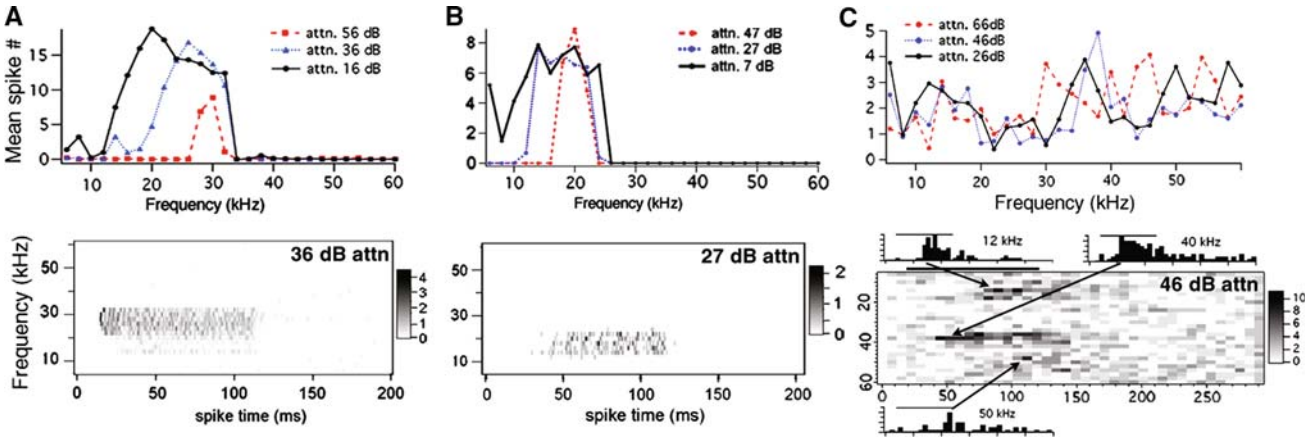


**Fig. 5** *Frequency tuning and Spectral-temporal histograms of identified units in awake mouse DCN.* **a** Fusiform cell frequency tuning curve at three intensities (*top plot*) and spectral-temporal histogram (*bottom panel*). In spectral–temporal histograms, both frequency and temporal information are retained with time on the *x*-axis and frequency of sound stimulation on the *y*-axis. Each row represents the PSTH for the corresponding frequency. **b** Vertical (type II, buildup) cell frequency tuning curve at three intensities (*top panel*) and spectral–temporal histogram (*bottom panel*). Cartwheel cell frequency response maps at three levels of intensity (*top panel*). The frequency tuning of this cartwheel cell is not easily distinguishable by the response map. Spectral–temporal histogram (*bottom panel*) with select PSTHs shown in detail (bin width = 7 ms). The unit shows an excitatory response to two separate frequency regions (12 and 40 kHz) with inhibition between. This frequency tuning for this cartwheel cell is only apparent in our spectral-temporal plot and not in commonly used response maps

frequency cannot be determined (Parham and Kim 1995; Parham et al. 2000). In contrast, we found that frequency tuning of many cartwheel cells was fairly sharp, but often complex so that response maps were not apparent when plotted in the traditional manner (Fig. 5c, top plot). However, frequency tuning of excitation and inhibition was much more apparent in some units when we generated spectral–temporal histograms (Fig. 5c, bottom plot). Preserving the temporal information in our spectral–temporal histograms allows changes in spike rate to be more easily distinguished compared to a standard response map. The spectral-temporal histogram in Fig. 5c, shows a long latency excitatory response to at least two different frequencies (12 and 40 kHz), tuning that was indistinguishable in the traditional response map. The mean (SD) minimum threshold for cartwheel cells was 33 (11) dB SPL, only slightly higher than the DCN units that receive direct input from auditory nerve afferents (Table 1). In contrast, other studies have found that cartwheel cells did not respond as strongly to tones, but agreed that the traditional tuning curves were complex enough to make the best frequency difficult to resolve (Parham and Kim 1995; Parham et al. 2000; Young and Davis 2002).

Since our results show that cartwheel cells in the awake mouse DCN respond well to pure tones, we can use auditory stimuli alone as an event that is consistently correlated with another auditory stimulus to test our hypothesis that adaptation to biologically relevant sounds occurs in the DCN. These results improve our understanding of how the DCN functions as an adaptive filter to aid animals in attending to important features of auditory objects. In addition, by extending our stimuli to include vocalizations, we can demonstrate that neurons in DCN process complex sounds that are behaviorally relevant to the animal.

### 4.2 Cartwheel cells show selective responses to mouse vocalizations

We have recorded and characterized the acoustic features of vocalizations emitted by normal hearing mice under different social and environmental conditions. Mice emit at least ten different types of vocalizations; half of which are frequency modulations (whistles) and the other half of which are complex with multiple frequency components and specific temporal features. The biological meaning of some of these calls is known. For example, during courtship male mice emit sequences of vocalizations that have been referred to as song (Holy and Guo 2005), in part due to the frequency and temporal structure of the vocalizations. In addition, pups emit specific calls to release different types of maternal behaviors. By characterizing the acoustic features of over 2000 mouse calls, we have generated a set of stereotypical vocalizations that we have used as stimuli to encompass the majority of complex vocalizations emitted by our mice under our social and environmental conditions. Figure 6 illustrates responses of a cartwheel cell in mouse DCN to a sample of our mouse vocalization stimuli. This cell responded to two of the 16 vocalizations we presented. These results show that cartwheel cells respond to complex sounds such as mouse vocalizations.

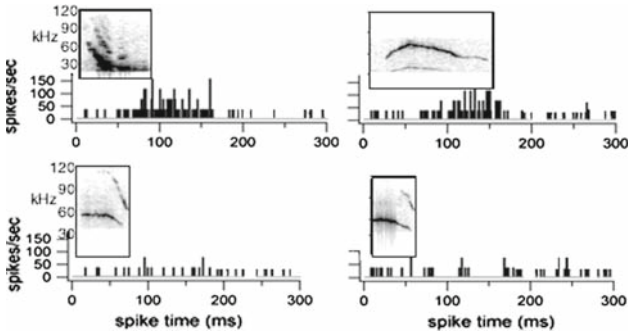


**Fig. 6** *Cartwheel cells respond to natural mouse vocalizations.* PSTHs elicited from four mouse vocalizations show that the cartwheel cell responded well to two of the calls. The inset in the PSTHs show the vocalization spectograms. The time scale for the spectogram and the PSTH in each plot is the same so that the spectograms shows the appropriate onset time and duration of the stimulus for the PSTH. Calls were recorded using a 1/4-inch condenser microphone, digitized at 333,000 samples/s, and analyzed using custom-written software. Plots of frequency versus time for all calls were obtained after fast Fourier transformation

In a complex auditory scene, a conspecific vocalization is a particularly important auditory object to localize. The fact that selectivity to specific vocalizations are made at this early level may be relevant to the function of DCN in forming a spectral-temporal coding of auditory objects that could be required for monaural sound localization (May 2000; Oertel and Young 2004; Rogers and Butler 1992).

### 4.3 Model of temporal characteristics of cartwheel cells in awake mouse DCN

Our purpose was to develop models of cartwheel cells that would predict auditory responses of complex spiking neurons recorded in the awake mouse (Portfors and Roberts 2007) in order to identify parallel fiber synaptic inputs. Our aim was to construct a more realistic cartwheel cell model than the spike response model (Gerstner et al. 1993) used in our previous studies of cerebellum-like structures (Roberts and Bell 2000). The model helped us to tease apart the effects due to intrinsic properties of cartwheel cells from the effects due to synaptic input patterns (Portfors and Roberts 2007). We constructed a 2-dimensional integrate-and-fire (2d-IF) model (Izhikevich 2003, 2006) that was based on the dynamics of the membrane currents. We used a dynamical systems approach (Izhikevich 2006) to reduce the model of a cartwheel cell to 2 variables, the membrane potential, $v$, and a slow "recovery" variable, $u$. In this type of model, a fast spike is initiated when the $v$-variable crosses a preset threshold, and the two variables are reset.

Cartwheel cells have 2 types of spikes: simple spikes and complex spikes. The complex spikes are driven by a slow, $Ca^{2+}$-based plateau (Manis et al. 1994; Zhang and Oertel 1993; Kim and Trussell. 2007). Fast, sodium-dependent spikes ride on top of the plateau potential (Golding and Oertel 1997), and the complex spike burst is presumably terminated by the activation of a calcium-dependent potassium current ($I_{\mathrm{AHP}}$). Using a dynamical systems approach, this type of burst mechanism leads to a fold/homoclinic bifurcation in Izhikevich's topological classification (Izhikevich 2006). During a burst, each fast cycle around the unstable focus (each spike) increments a slow, recovery variable that eventually repolarizes the cell and terminates the burst. We represented the bursting dynamics with a 2-state, resetting (integrate-and-fire) model:

$$C_m \dot{v} = k(v_r - v)(v_t - v) - u + I \tag{7}$$

$$\dot{u} = a(b(v - v_r) - u) \tag{8}$$

If $v \geq v_{peak}$, then $v \rightarrow c$, and $u \rightarrow u + d$. To simulate cartwheel cell spiking dynamics, the parameters were set to the following values: $C_m = 50\,\mathrm{pF}$, $v_r = -65\,\mathrm{mV}$, $v_t = -35\,\mathrm{mV}$, $k = 1$, $v_{\mathrm{peak}} = 0\,\mathrm{mV}$, $a = 0.03$, $b = 10$, $c = -40$, $d = 100$, and the variables are initiated at equilibrium ($v = -65\,\mathrm{mV}$ and $u = 0\,\mathrm{nA}$) (Portfors and Roberts 2007).

Synaptic inputs to the 2d-IF models were represented as postsynaptic currents, $I_s(t) = g_s(t)(V(t) - E_r)$, where $E_r$ is the reversal potential, and the synaptic conductance, $g_s(t) = g_{\max} r(t)$, where $r(t)$ represented the open probability of synaptic channels. We used a linear Markov model for calculating $r(t)$ with a single-variable (2-states, open and closed) model for AMPA receptors, and $r(t)$ was described by the equation, $\dot{r} = \alpha T(1-r) - \beta r$. The transmitter variable $T$ was reset $T \rightarrow T_{\max}$ only if there is a presynaptic spike, otherwise, $T = 0$ ($T_{\max} = 0.1$ and $E_r = 0\,\mathrm{mV}$).

A series of synaptic currents were injected into the model cartwheel cell to represent parallel fiber activity that results from auditory stimulation. The maximum synaptic current was graded throughout the stimulus cycle to represent the temporal pattern of synaptic currents. Thus, when we match the complex and simple spike pattern with a cartwheel cell recorded *in vivo*, we arrive at a prediction of the synaptic currents that generated the spike pattern.

Simulated cartwheel cell spike patterns are shown in Fig. 7b. The only difference between these two models was the peak of the synaptic current. The model cartwheel cell responded with long-latency complex spikes followed by simple spikes. The spike patterns (Fig. 7b) are consistent with our recordings of cartwheel cells in the awake mouse (Fig. 7a). This modeling study suggests that cartwheel cell spike patterns during auditory stimuli are due to synaptic inputs, but the observed temporal relationship between complex and simple spikes is due to membrane properties of cartwheel cells. In addition, the model suggests that parallel fibers carry delayed information about the frequency composition of sounds that generate responses in cartwheel cells.

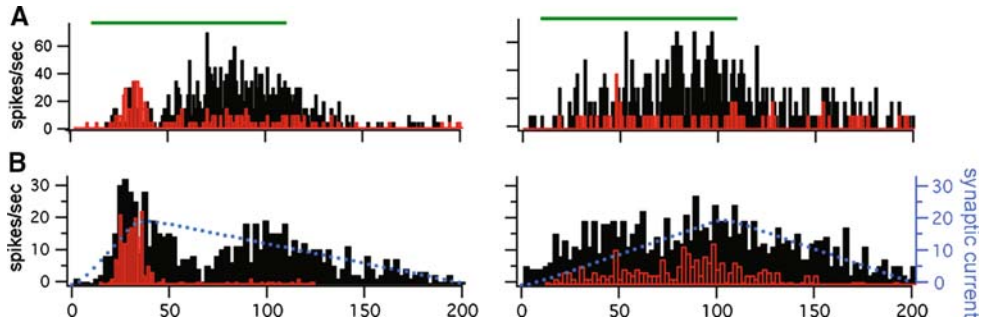


**Fig. 7** *Simulation of a 1-compartment, 2-dimensional, integrate-and-fire cartwheel cell reveals mechanisms of spike pattern as recorded in vivo.* **a** Poststimulus time histograms show temporal firing patterns of complex (CS) and simple spikes (SS) to 200 presentations of the characteristic frequency at 30 dB above threshold (bin width = 3ms). *Red* (*grey*), open bars plot CS and black bars plot SS. Horizontal bars in raster plots and PSTHs show onset and duration of the sound stimulus. Characteristic frequency and threshold were 16 kHz and 25 dB SPL for the unit in the left panel and 32 kHz and 25 dB SPL for the unit in the right panel. CSs were differentiated from SSs based on interspike interval time. Note the long latencies and variability in the timing of the first spike latency in both units. **b** A series of excitatory postsynaptic currents (*dotted blue*) leads to early complex spikes (red) and late simple spikes (*black*). Repeated presentations of the synaptic current leads to spiking pattern that resembles auditory responses of cartwheel cells in vivo. Histogram shows a dominance of complex spikes early in the cycle depends on the peak of the series of synaptic inputs

These delays can now be implemented in our model of adaptive learning in cartwheel cells that results from STDP.

### 4.4 Adaptive model of cartwheel response to auditory stimuli

Synaptic plasticity in cartwheel cells is dependent on the time between the parallel fiber spike and the postsynaptic spike (Tzounopoulos et al. 2004). Previous mathematical modeling of anti-Hebbian STDP has established a globally stable fixed point in the learning dynamics (Roberts et al. 2006a). The STDP learning rule for the synapse from PFs onto cartwheel cells is anti-Hebbian, and we simulated how cartwheel cell responses to a tone changes as a result of pairing one tone with a different tone (Roberts et al. 2006b). The simulation motivated an experimental test that supported the expectation of the simulation. We then tested and confirmed the model-driven hypothesis that pairing two sounds induces cartwheel cells to change their response to each individual sound such that the response to one sound cancels the effect of adding the second sound (Fig. 8).

Our simulation consisted of two components: a granule cell network, and a cartwheel cell. The granule cell network distributed an auditory stimulus via a recurrent network onto the model cartwheel cell (Roberts 2004, 2005). The model cartwheel cell implemented a STDP learning rule at the parallel fiber inputs that was consistent with recent empirical data (Tzounopoulos et al. 2004) (Fig. 4b). A spike-response model was used to represent the cartwheel cell, and two types of spikes were generated representing simple and complex spikes. As with our previous studies in the electrosensory lateral line lobe (Roberts and Bell 2000; Roberts 2000; Roberts and Bell 2002; Roberts 2005; Williams et al. 2003; Roberts et al. 2006a), the anti-Hebbian STDP learning rule drove the output rate of the cartwheel cell to a fixed point determined by the parameters of the learning rule.

The model was initialized with parallel fiber synaptic weights at their maximum and then allowed to approach their equilibrium value for stimulus-1 (cycle time: 0–150 ms). Then, the second set of mossy fibers were activated to represent stimulus-2 (cycle time: 50–150 ms). The increased cartwheel cell spike rate (Fig. 8a) depressed all the active parallel fiber synaptic weights. When stimulus-2 was terminated, the spike response to stimulus-1 was reduced below the values prior to the pairing with stimulus-2 for the cycle-interval following the onset of stimulus-2. Thus, the model predicted that the pairing of two stimuli reduces the response to the first stimulus for the interval following the onset of the second stimulus.

### 4.5 Observed adaptation of cartwheel cell responses to auditory stimuli confirms the model's prediction

We tested our model's prediction in our awake mouse preparation by recording the spiking activity of cartwheel cells during the pairing of two different tones. Stimulus-1 was not the best frequency, but would act as a reference to activate a population of granule cells. Stimulus-2 was a best frequency tone that evoked a strong excitatory response (Fig. 8b). After repeated pairing of the 2 stimuli for about 5 mins (1,000 presentations at 3 per sec) the spike response to stimulus-2 was reduced, in particular, the simple spikes were significantly reduced (Fig. 8c, Appendix for description of KS-test). After stimulus-2 was terminated, the simple spike response to stimulus-1 was significantly reduced during the period following the expected onset of stimulus-2. Thus, we have

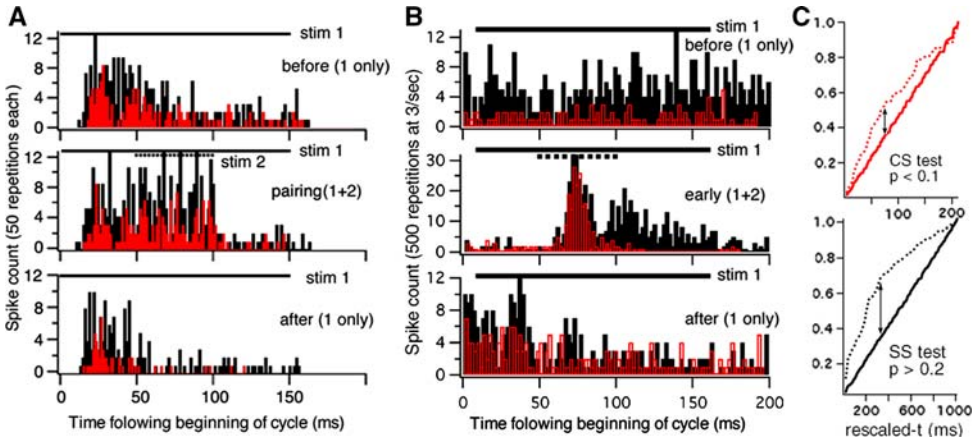


**Fig. 8** *Cartwheel cell's response to a tone changes following pairing with a second tone: model versus experiment.* **a** Simulated adaptation of a model cartwheel cell that receives parallel fiber input from a granule cell network, and the STDP learning rule from (Tzounopoulos et al. 2004) (Fig. 4b). **b** Extracellular spike recordings of a cartwheel cell in an awake mouse support the prediction (bin width = 2 ms). Complex spikes in *red* (*grey*) and simple spikes in black. **c** KS-test for adaptation of the complex and simple spikes (data from B, 500 repetitions) shows that the complex spikes (*top panel*) do not adapt when comparing the time-rescaled PSTHs for before (*solid*) and after (*dotted*) the pairing (significance level: $\alpha = 0.1$), but there is significant adaptation in the simple spikes (*bottom panel*)

empirically confirmed our model-driven hypothesis that the pairing of two tones reduces the response of cartwheel cells to individual tones.

### 4.6 Model of frequency response of fusiform cells

The purpose of this study was to develop a network model of the DCN based on spectral models of type III/IV cells (Blum and Reed 1998; Hancock and Voigt 1999; Reiss and Young 2005). The resultant model predicts the responses of fusiform cells to vocalizations from which we can infer the system level effects of synaptic plasticity. In the initial phase of the model, we chose synaptic connections that minimized the difference between the model prediction and data from extracellular recordings in the awake mouse. The remaining differences were then identified and suggest mechanisms that would improve the agreement between the model and experimental results.

The network consisted of three neuronal types: fusiform (fusiform) cells (P), type-II inhibitory interneurons (I2), and wide-band inhibitory interneurons shown in Fig. 9a. The frequency responses of the network were driven by a model on the auditory nerve (AN) responses. The AN model was based on a modified version of Carney's AN model (Carney 1993; Zhang et al. 2001; Nelson and Carney 2004) where we shifted the frequency range and response properties to mimic AN responses in the mouse (Taberner and Liberman 2005). In our simulation, the AN filter bank responded to the stimulus with 10 fibers each tuned through the range of 1–30 kHz.

A narrow-band synaptic connection from the AN model to the fusiform cell (P) was represented as an alpha-function convolved with the spike probability of each AN fiber to represent an excitatory postsynaptic potential (EPSP), and a bell-shaped frequency distribution. The model network implemented 10 wide-band inhibitory interneurons (W) by a delayed (disynaptic) inhibitory postsynaptic potential (IPSP) convolved with the AN spike probability. Ten type II (I2) neurons received excitation from the AN and inhibition from W (Blum and Reed 1998; Hancock and Voigt 1999; Reiss and Young 2005). All 21 neurons received a bell-shaped distribution of synaptic inputs from the AN, and P received bell-shaped distributed inputs from I2 and W across the tonotopy induced by the AN model.

The response of the model was modified by adjusting the strength and the band-width of the synaptic connections by an exhaustive search strategy to minimize the difference between the spectral–temporal histograms of the P-cell (Fig. 9b) and the experimental recording (Fig. 9c).

Following model optimization, we performed a statistical test to determine if the spike response, simulated by the model, significantly differed from the recorded PSTH. To compare the *shape* of the data and model PSTHs, we used a Kolmogorov–Smirnov (KS) test (see Appendix). The errors in the model suggest mechanisms involved in the processing of auditory information in DCN. By comparing the spectral–temporal histograms in Fig. 9b and c, the model errors include three prominent features: (1) Inhibitory sidebands should be more prominent at the higher stimulus intensity level (42 dB SPL). (2) There should be a rhythmic spike rate near the best frequency that is at a much lower frequency than the

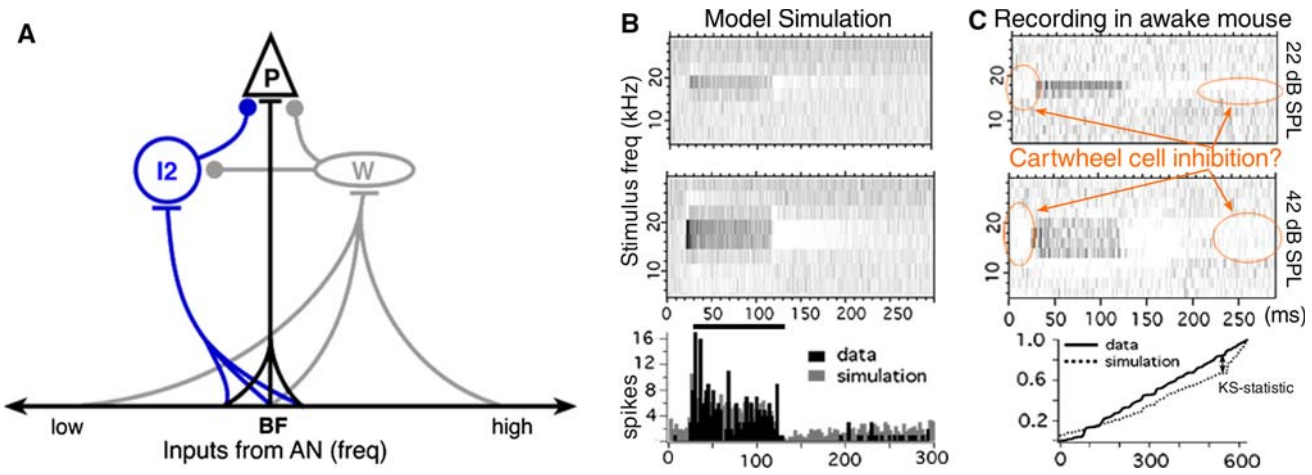


**Fig. 9** *Our network model of fusiform cell responses reveals missing mechanisms when compared with our experimental results.* **a** The network contained an auditory nerve (AN) model modified from (Nelson and Carney 2004). The model fusiform cell (P) received synaptic input from the AN, an array of 10 wide-band, inhibitory interneurons (W), and an array of 10 type II units (I2). The type II units received inhibition from W and inhibited P (Blum and Reed 1998; Hancock and Voigt 1999; Reiss and Young 2005). **b** The model results for a set of pure-tone stimulations at 10 frequencies 1–30 kHz, and for two amplitudes (22–42 dB SPL). The spectral–temporal PSTHs show a sharp AN-like onset, lateral inhibition, and a reduction in the spontaneous rate following the stimulus due to forward masking in the auditory nerve response. Bottom panel shows overlay of the simulation and data PSTHs for 20 kHz at 22 dB SPL. **c** Data from single unit recording in DCN of an awake mouse that were used to tune the model. The long-lasting inhibition that follows the evoked response may be due to cartwheel cell inhibitory inputs. **d** Kolmogorov–Smirnov (KS) test of the time-rescaled cumulative spike probability functions for the data and the simulation (20 kHz, 22 dB SPL). The test rejects the simulation as the null hypothesis with $p > 0.1$

stimulus. (3) The spontaneous activity should be inhibited *before* the stimulus presentation near the best frequency.

These identified errors in the model's predictions suggest mechanisms that could lead to a better agreement by extending the model with (1) more realistic spiking mechanism in our model of W, (2) more realistic membrane properties for F to generate oscillations (Golding and Oertel 1997; Ding et al. 1999; Manis et al. 1994; Kanold and Manis 2001), and (3) include cartwheel cells in the network to induce late inhibition of P. The value if this approach is that the model can be used to develop new experimental protocols that would specifically probe the hypotheses generated by each stage of modeling.

## 5 Design principles of the ELL and DCN

The anatomical similarities of these two cerebellum-like structure lead to functional principles of their design. This review of these structures suggests to the following design principles:

1. Each contains a set of sensory relay units (LG and LF cells in ELL and fusiform cells in DCN) that represent characteristics of the objects in each sensory modality by the unit's position: somatotopy in ELL and tonotopy in DCN.
2. The sensory relay units receive a large number of temporally distributed inputs (parallel fibers) to provide both timing information and "context" information.
3. The sensory relay units also receive an inhibitory input from neurons that decorrelate repeated associations with parallel fiber information.
4. Synaptic learning rules at the parallel fiber synapses appear to be tailored to the types of objects that will be processed by each sensory modality.

The cerebellum-like structures do not themselves encode object location, but process sensory information so that objects particular to the sensor modality can be readily identified and classified. The type of processing that appears to take place in these examples appears to be to amplify important and defining characteristics of external objects and reduce redundancies and noise in the sensory environment.

## 6 Functional consequences of the differences between the designs of the ELL and DCN

The adaptive properties of Purkinje-like neurons in the DCN are strikingly similar to Purkinje-like neurons in the ELL. As in the ELL, DCN-neurons reduce their response to a sensory pattern suggesting that a similar biological principle may be

at work. However, since different types of objects are processed by the DCN neurons, one would expect a different type of adaptation system. The salient question that arises is: what do the differences in structure and physiology between ELL and DCN imply for the differences in how sensory objects are analyzed?

Three key differences between ELL and DCN guide us to a parsimonious explanation: (1) The lack of a corollary discharge in the auditory system to notify the DCN of when an externally generated sound begins. (2) There are no direct auditory nerve input to the Purkinje-like neurons in the DCN. (3) The efferent neurons of DCN have a different STDP learning rule.

The first difference suggests that adaptation to externally generated sounds during passive listening by the animal preclude the possibility of centrally originating signals such as a corollary discharge. Thus, the auditory stimulus itself must generate the timing signals.

The effects of the second difference between ELL and DCN are seen in Fig. 9b, c. In the ELL, the MG cells regulate the output of the system on an immediate basis, thereby cancelling predictable signals with a very short latency. In DCN, the effects of cartwheel cells on the efferent cells are slow and late. The likely cartwheel cell influence on fusiform cells is not fast enough to affect the response to a single, short sound. The function, therefore, must regulate a stream of auditory stimulation in order to modify the spectral predictability of a temporal scene. The result may be to dampen background noise that contains a predictable frequency structure.

The third difference between ELL and DCN, that the efferent cells have a different STDP learning rule, cannot be underestimated. Although the efferent cells in ELL have been demonstrated to express some STDP learning at the parallel fiber input (Han et al. 2000), this plasticity is weak compared to MG cells and it is anti-Hebbian like the MG cells. The STDP learning rule at the parallel fiber synapse onto fusiform cells in DCN is Hebbian and increases temporal correlations between different inputs. Rather than amplifying novel inputs, the fusiform cell will group frequencies that consistently appear together, ie. amplify the frequency structure of familiar auditory objects.

In the ELL, the edges of objects can be accentuated by lateral inhibition because the electrical shadow cast by objects in the environment always have a clear, spatial structure. However, auditory objects do not have such an a priori structure, but must be learned to be recognized. Recent evidence suggests that the DCN can act as an auditory edge detector (Reiss and Young 2005). The Hebbian STDP learning rule has the dynamics that could lead to temporal edge amplification within each frequency band. Thus, the types of objects that each cerebellum-like structure is designed to analyze has directed the design principles that that have been expressed in their functional circuits.

**Acknowledgments** The authors would like to thank Curt Bell for an exciting collaboration and helpful suggestions on the manuscript.

## Appendix: Time-rescaled Kolmogorov–Smirnov (KS) test

Interpreting the PSTH as a spike probability function could lead to false conclusions because the PSTH is not a normalized probability density. However, we can apply the time-rescaling theorem (Brown et al. 2002) to convert the spike latencies of any point process to a Poisson process of unit rate. The transformation of the recorded PSTH then becomes our standard to compare with the simulated PSTH.

To apply the KS-test, we time-rescaled the experimental spike latencies, $t_i$ to latencies of a Poisson process, $\tau_i$, using the transformation, $\tau_i = \int_0^{t_i} f(t)\mathrm{d}t$, where $f(t)$ is the instantaneous probability of a spike at time $t$. We used the experimental PSTH divided by the number of trials to estimate the function $f(t)$. The resulting histogram of transformed latencies will be constant, and the cumulative functions is the solid line shown in Fig. 9d. We then time-rescaled the latencies of the simulated spike responses, *using the experimental PSTH*, so that the rescaling will show the difference between the simulation and experiment. We applied the two-sided KS-test in the fusiform model (Fig. 9d), with the KS-statistic, $\max |\mathrm{CDF}_{\mathrm{expr}}(\tau) - \mathrm{CDF}_{\mathrm{simul}}(\tau)| = 0.21$, where the functions $\mathrm{CDF}_{\mathrm{expr}}(\tau)$ and $\mathrm{CDF}_{\mathrm{simul}}(\tau)$ are the cumulative histograms of the transformed latencies shown in Fig. 9d. We had 25 samples in the experimental data, so we compute $p > 0.1$, which is greater than an acceptable level of significance. We therefore reject the model as a quantitative hypothesis.

## References

Abbott LF, Nelson SB (2000) Synaptic plasticity: taming the beast. Nature Neurosci 3(Suppl):1178–1183

Albus JS (1971) A theory of cerebellar function. Math Biosci 10:25–61

Bastian J (1996) Plasticity in an electrosensory system. II. Postsynaptic events associated with a dynamic sensory filter. J Neurophysiol 76:2497–2507

Bell CC (1981) An efference copy in electric fish. Science 214:450–453

Bell CC (1989) Sensory coding and corollary discharge effects in mormyrid electric fish. J Exp Biol 146:229–253

Bell CC, Grant K, Serrier J (1992) Sensory processing and corollary discharge effects in the mormyromast regions of the mormyrid electrosensory lobe: I. Field potentials and cellular activity in associated structures. J Neurophysiol 68:843–858

Bell CC, Caputi A, Grant K, Serrier J (1993) Storage of a sensory pattern by anti-Hebbian synaptic plasticity in an electric fish. Proc Natl Acad Sci USA 90:4650–4654

Bell CC, Bodznick D, Montgomery J, Bastian J (1997b) The generation and subtraction of sensory expectations within cerebellum-like structures. Brain Beh Evol 50(Suppl. 1):17–31

Bell CC, Han V, Sugawara Y, Grant K (1997b) Synaptic plasticity in a cerebellum-like structure depends on temporal order. Nature 387:278–281

Beroukha A, Gruen E, Woody CD (1998) Facilitation of acoustic responses of cartwheel neurons of the cat dorsal cochlear nucleus. Neuroreport 9(15):3457–3461

Berrebi AS, Mugnaini E (1991) Distribution and targets of the cartwheel cell axon in the dorsal cochlear nucleus of the guinea pig. Anat Embryol (Berl) 183(5):427–454

Blum JJ, Reed MC (1998) Effects of wide band inhibitors in the dorsal cochlear nucleus. ii. model calculations of the responses to complex sounds. J Acoust Soc Am 103(4):2000–2009

Bodznick D, Montgomery JC, Bradley DJ (1992) Suppression of common mode signals within the electrosensory system of the little skate Raja erinacea. J Exp Biol 171:107–125

Brown EN, Barbieri R, Ventura V, Kass RE, Frank LM (2002) The time-rescaling theorem and its application to neural spike train data analysis. Neural Comput 14(2):325–346

Brown M, Berglund A, Kiang N, Ryugo D (1988) Central trajectories of type ii spiral ganglion neurons. J Comp Neurol 278: 581–590

Caicedo A, Herbert H (1993) Topography of descending projections from the inferior colliculus to auditory brainstem nuclei in the rat. J Comp Neurol 328:377–392

Caputi AA, Budelli R (2006) Peripheral electrosensory imaging by weakly electric fish. J Comp Physiol A Neuroethol Sens Neural Behav Physiol 192(6):587–600

Caputi AA, Budelli R, Grant K, Bell CC (1998) The electric image in weakly electric fish: physical images of resistive objects in gnathonemus petersii. J Exp Biol 201:2115–2128

Carney LH (1993) A model for the responses of low-frequency auditory-nerve fibers in cat. J Acoust Soc Am 93(1):401–417

Chen C, Thompson RF (1995) Temporal specificity of long-term depression in parallel fiber-Purkinje synapses in rat cerebellar slices. Learn Memory 2:185–198

Coesmans M, Weber JT, Zeeuw CID, Hansel C (2004) Bidirectional parallel fiber plasticity in the cerebellum under climbing fiber control. Neuron 44(4):691–700

Crick F (1984) Function of the thalamic reticular complex: the searchlight hypothesis. Proc Natl Acad Sci USA 81:4586–4590

Davis KA, Gdowski GT, Voigt HF (1995) A statistically based method to generate response maps objectively. Journal of Neuroscience Methods 57(1):107–118

Davis KA, Ding J, Benson TE, Voigt HF (1996a) Response properties of units in the dorsal cochlear nucleus of unanesthetized decerebrate gerbil. J Neurophysiol 75(4):1411–1431

Davis KA, Miller RL, Young ED (1996b) Effects of somatosensory and parallel-fiber stimulation on neurons in dorsal cochlear nucleus. J Neurophysiol 76(5):3012–3024

Ding J, Benson TE, Voigt HF (1999) Acoustic and Current-Pulse Responses of Identified Neurons in the Dorsal Cochlear Nucleus of Unanesthetized, Decerebrate Gerbils. J Neurophysiol 82(6):3434–3457

von der Emde G, Schwarz S, Gomez L, Budelli R, Grant K (1998) Electric fish measure distance in the dark. Nature 395(6705):890–894

Evans E, Nelson P (1973) The responses of single neurones in the cochlear nucleus of the cat as a function of their location and the anaesthetic state. Exp Brain Res 17:402–427

Franosch JM, Kempter R, Fastl H, van Hemmen JL (2003) Zwicker tone illusion and noise reduction in the auditory system. Phys Rev Lett 90(17):178, 103

Frisina RD, Walton JP, Karcich KJ (1994) Dorsal cochlear nucleus single neurons can enhance temporal processing capabilities in background noise. Exp Brain Res 102(1):160–164

Fujino K, Oertel D (2003) Bidirectional synaptic plasticity in the cerebellum-like mammalian dorsal cochlear nucleus. Proc Natl Acad Sci USA 100(1):265–270

Gerstner W, Ritz R, Hemmen JLvan (1993) Why spikes? Hebbian learning and retrieval of time-resolved excitation patterns. Biol Cybern 69:503–515

Godfrey D, Kiang N, Norris B (1975) Single unit activity in the dorsal cochlear nucleus of the cat. J Comp Neurol 162:269–284

Golding N, Oertel D (1997) Physiological identification of the targets of cartwheel cells of the dorsal cochlear nucleus. J Neurophysiol 78:248–260

Golding NL, Robertson D, Oertel D (1995) Recordings from slices indicate that octopus cells of the cochlear nucleus detect coincident firing of auditory nerve fibers with temporal precision. J Neurosci 15(4):3138–3153

Gomez L, Budelli R, Grant K, Caputi AA (2004) Pre-receptor profile of sensory images and primary afferent neuronal representation in the mormyrid electrosensory system. J Exp Biol 207(Pt 14):2443–2453

Haenggeli, Pongstaporn T, Doucet J, Ryugo D (2005) Projections from the spinal trigeminal nucleus to the cochlear nucleus in the rat. J Comparative Neurol 484(2):191–205

Han V, Bell CC, Grant K, Sugawara Y (1999) Mormyrid electrosensory lobe in vitro: I. Morphology of cells and circuits. J Comp Neurol 404:359–374

Han V, Grant K, Bell CC (2000) Reversible associative depression and nonassociative potentiation at a parallel fiber synapse. Neuron 27:611–622

Hancock KE, Voigt HF (1999) Wideband inhibition of dorsal cochlear nu- cleus type iv units in cat: a computational model. Ann Biomed Eng 27:73–87

Harvey RJ, Napper RM (1991) Quantitative studies on the mammalian cerebellum. Prog Neurobiol 36:437–463

Holy TE, Guo Z (2005) Ultrasonic songs of male mice. PLoS Biol 3(12):e386

Izhikevich EM (2003) Simple model of spiking neurons. IEEE Trans Neural Networks 14:1569–1572

Izhikevich EM (2006) Dynamical systems in neuroscience: the geometry of excitability and bursting. MIT Press, Cambridge, MA

Jenkins WM, Masterton RB (1982) Sound localization: effects of unilateral lesions in central auditory system. J Neurophysiol 47(6):987–1016

Kaltenbach J, Saunders J (1987) Spectral and temporal response patterns of single units in the chinchilla dorsal cochlear nucleus. J Exp Neurol 96:406–419

Kaltenbach JA, Meleca RJ, Falzarano PR, Myers SF, Simpson TH (1993) Forward masking properties of neurons in the dorsal cochlear nucleus: possible role in the process of echo suppression. Hear Res 67(1–2):35–44

Kanold PO, Manis PB (2001) A physiologically based model of discharge pattern regulation by transient k+ currents in cochlear nucleus pyramidal cells. J Neurophysiol 85(2):523–538

Karachot L, Kado RT, Ito M (1994) Stimulus parameters for induction of long-term depression in *in vitro* rat Purkinje cells. Neurosci Res 21:161–168

Kim Y, Trussell LO (2007) Ion channels generating complex spikes in cartwheel cells of the dorsal cochlear nucleus. J Neurophysiol 97(2):1705–1725

Lev-Ram V, Makings LR, Keitz PF, Kao JPY, Tsien RY (1995) Long-term depression in cerebellar Purkinje neurons results from coincidence of nitric oxide and depolarization-induced $Ca^{2+}$ transients. Neuron 15:407–415

Lev-Ram V, Wong ST, Storm DR, Tsien RY (2002) A new form of cerebellar long-term potentiation is postsynaptic and depends on nitric oxide but not camp. Proc Natl Acad Sci USA 99(12):8389–8393

Li H, Mizuno N (1997) Single neurons in the spinal trigeminal and dorsal column nuclei project to both the cochlear nucleus and

the inferior colliculus by way of axon collaterals: a fluorescent retrograde double-labeling study in the rat. Neuroscience Research 29(2):135–142

Linden DJ, Connor JA (1993) Cellular mechanisms of long-term depression in the cerebellum. Curr Op Neurobiol 3:401–406

Manis PB, Spirou GA, Wright DD, Paydar S, Ryugo DK (1994) Physiology and morphology of complex spiking neurons in the guinea pig dorsal cochlear nucleus. J Comp Neurol 348(2):261–276

Marr D (1969) A theory of cerebellar cortex. J Physiol 202:437–470

May BJ (2000) Role of the dorsal cochlear nucleus in the sound localization behavior of cats. Hear Res 148(1–2):74–87

Medina JF, Mauk MD (2000) Computer simulation of cerebellar information processing. Nat Neurosci 3(Suppl):1205–1211

Mohr C, Roberts PD, Bell CC (2002a) Cells of the mormyrid electrosensory lobe: I. Responses to the electric organ corollary discharge and to electrosensory stimuli. J Neurophysiol 90:1193–1210

Mohr C, Roberts PD, Bell CC (2002b) Cells of the mormyrid electrosensory lobe: II. Responses to input from central sources. J Neurophysiol 90:1211–1223

Montgomery JC, Bodznick D (1994) An adaptive filter that cancels self-induced noise in the electrosensory and lateral line mechanosensory systems of fish. Neurosci Letters 174:145–148

Nelson ME, Paulin MG (1995) Neural simulations of adaptive reafference suppression in the elasmobranch electrosensory system. J Comp Physiol A 177:723–736

Nelson PC, Carney LH (2004) A phenomenological model of peripheral and central neural responses to amplitude-modulated tones. J Acoust Soc Am 116(4 Pt 1):2173–86

Oertel D, Young ED (2004) What's a cerebellar circuit doing in the auditory system. Trends Neurosci 27:104–110

Ohlrogge M, Doucet J, Ryugo D (2001) Projections of the pontine nuclei to the cochlear nucleus in rats. J Comp Neurol 436:290–303

Osen K (1969) Cytoarchitecture of the cochlear nuclei in cat. J Comp Neurol 136:453–484

Parham K, Kim DO (1995) Spontaneous and sound-evoked discharge characteristics of complex-spiking neurons in the dorsal cochlear nucleus of the unanesthetized decerebrate cat. J Neurophysiol 73(2):550–561

Parham K, Bonaiuto G, Carlson S, Turner JG, R DW, Bross LS, Fox A, Willott JF, Kim DO (2000) Purkinje cell degeneration and control mice: responses of single units in the dorsal cochlear nucleus and the acoustic startle response. Hearing Research 148(1–2):137–152

Pfeiffer R (1966) Classification of response patterns of spike discharges for units in the cochlear nucleus: tone burst stimulation. Exp Brain Res 1:220–235

Portfors CV, Roberts PD (2007) Temporal and frequency characteristics of cartwheel cells in the awake mouse dcn, J Neurophysiol (June 20, Epub)

Reiss LAJ, Young ED (2005) Spectral edge sensitivity in neural circuits of the dorsal cochlear nucleus. J Neurosci 25:3680–3691

Rhode W, Smith P, Oertel D (1983) Physiological response properties of cells labeled intracellularly with horseradish peroxidase in cat dorsal cochlear nucleus. J Comp Neurol 213:426–447

Rhode WS, Kettner RE (1987) Physiological study of neurons in the dorsal and posteroventral cochlear nucleus of the unanesthetized cat. J Neurophysiol 57(2):414–442

Rhode WS, Smith PH (1986) Physiological studies on neurons in the dorsal cochlear nucleus of cat. J Neurophysiol 56(2):287–307

Roberts PD (1999) Computational consequences of temporally asymmetric learning rules: I. Differential Hebbian learning. J Comput Neurosci 7:235–246

Roberts PD (2000) Dynamics of temporal learning rules. Phys Rev E 62:4077–4082

Roberts PD (2004) Recurrent biological neural networks: The weak and noisy limit. Phys Rev E 69:031, 910

Roberts PD (2005) Recurrent neural network generates a basis for sensory image cancellation. Neurocomputing 65(66):237–242

Roberts PD (2007) Stability of complex spike timing-dependent plasticity in cerebellar learning. J Comput Neurosci 22(3):283–96

Roberts PD, Bell CC (2000) Computational consequences of temporally asymmetric learning rules: II. Sensory image cancellation. J Comput Neurosci 9:67–83

Roberts PD, Bell CC (2002) Spike timing dependent synaptic plasticity in biological systems. Biol Cybern 87:392–403

Roberts PD, Lafferriere G, Sawtell N, Williams A, Bell CC (2006a) Dynamic regulation of spike-timing dependent plasticity in electrosensory processing. Neurocomputing 69:1195–1198

Roberts PD, Portfors CV, Sawtell N, Felix R (2006b) Model of auditory prediction in the dorsal cochlear nucleus via spike-timing dependent plasticity. Neurocomputing 69:1191–1194

Rogers ME, Butler RA (1992) The linkage between stimulus frequency and covert peak areas as it relates to monaural localization. Percept Psychophys 52(5):536–546

Ryugo D, Willard F (1985) The dorsal cochlear nucleus of the mouse: a light microscopic analysis of neurons that project to the inferior colliculus. J Comp Neurol 242:381–396

Sawtell NB, Williams A (2008) Transformations of electrosensory encoding associated with an adaptive filter. J Neurosci 28(7):1598–1612

Sawtell NB, Williams A, Bell CC (2007) Central control of dendritic spikes shapes the responses of purkinje-like cells through spike timing-dependent synaptic plasticity. J Neurosci 27(7):1552–1565

Schofield B, Cant NB (1999) Descending auditory pathways: Projections from the inferior colliculus contact superior olivary cells that project bilaterally to the cochlear nuclei. The Journal of Comparative Neurology 409(2):210–223

Shofner WP, Young ED (1985) Excitatory/inhibitory response types in the cochlear nucleus: relationships to discharge patterns and responses to electrical stimulation of the auditory nerve. J Neurophysiol 54(4):917–939

Shore S, Vass Z, Wys N, Altschuler R (2000) Trigeminal ganglion innervates the auditory brainstem. J Comp Neurol 419:271–285

Shore SE (2005) Multisensory integration in the dorsal cochlear nucleus: unit responses to acoustic and trigeminal ganglion stimulation. Eur J Neurosci 21(12):3334–3348

Smith P, Rhode W (1989) Structural and functional properties distinguish two types of multipolar cells in the ventral cochlear nucleus. J Comp Neurol 282:595–616

Taberner AM, Liberman MC (2005) Response properties of single auditory nerve fibers in the mouse. J Neurophysiol 93(1):557–569

Thompson GC, Masterton RB (1978) Brain stem auditory pathways involved in reflexive head orientation to sound. J Neurophysiol 41(5):1183–1202

Tzounopoulos T, Kim Y, Oertel D, Trussell LO (2004) Cell-specific, spike timing-dependent plasticities in the dorsal cochlear nucleus. Nat Neurosci 7:719–725

Weedman DL, Ryugo DK (1996) Projections from auditory cortex to the cochlear nucleus in rats: synapses on granule cell dendrites. J Comp Neurol 371(2):311–324

Wickesberg RE, Oertel D (1990) Delayed, frequency-specific inhibition in the cochlear nuclei of mice: a mechanism for monaural echo suppression. J Neurosci 10(6):1762–1768

Williams A, Roberts PD, Leen TK (2003) Stability of negative-image equilibria in spike-timing-dependent plasticity. Phys Rev E 68(2–1):021, 923

Woody CD, Wang XF, Gruen E, Landeira-Fernandez J (1992) Unit activity to click cs changes in dorsal cochlear nucleus after conditioning. Neuroreport 3(5):385–388

Wouterlood F, Mugnaini E (1984) Cartwheel neurons of the dorsal cochlear nucleus: a golgi-electron microscopic study in rat. J Comp Neurol 227:136–157

Wouterlood F, Mugnaini E, Osen K, Dahl A (1984) Stellate neurons in rat dorsal cochlear nucleus studies with combined golgi impregnation and electron microscopy: synaptic connections and mutual coupling by gap junctions. J Neurocytol 13:639–664

Young ED (1984) Response characteristics of neurons of the cochlear nuclei. In: Berlin CI (ed) Hearing science, recent advances. College Hill, San Diego, pp 423–460

Young ED, Brownell WE (1976) Responses to tones and noise of single cells in dorsal cochlear nucleus of unanesthetized cats. J Neurophysiol 39(2):282–300

Young ED, Davis KA (2002) Circuitry and function of the dorsal cochlear nucleus. In: Oertel D, Fay R, Popper A (eds) Integrative functions in the mammalian auditory pathway. Springer, New York, pp 160–206

Young ED, Voigt HF (1982) Response properties of type ii and type iii units in dorsal cochlear nucleus. Hear Res 6:153–169

Young ED, Nelken I, Conley RA (1995) Somatosensory effects on neurons in dorsal cochlear nucleus. J Neurophysiol 73(2):743–765

Zhang S, Oertel D (1993) Cartwheel and superficial stellate cells of the dorsal cochlear nucleus of mice: intracellular recordings in slices. J Neurophysiol 69(5):1384–1397

Zhang X, Heinz MG, Bruce IC, Carney LH (2001) A phenomenological model for the responses of auditory-nerve fibers: I. nonlinear tuning with compression and suppression. J Acoust Soc Am 109(2):648–670

Zheng X, Voigt HF (2006) A modeling study of notch noise responses of type iii units in the gerbil dorsal cochlear nucleus. Ann Biomed Eng 34(4):697–708